Investigation of 2D Materials Effect on Few-Mode Fiber Optical Temperature and Strain Sensors

Morteza Janfaza[a], Hamed Moradi[b,*], and Morteza Maleki[c]

[a]Faculty of Engineering, Electrical Engineering Department, Jahrom University, Jahrom, Iran
[b]Physics Department, Amirkabir University of Technology, Tehran, Iran
[c]RF MEMS and Bio-Nano-Electronics Lab, Electrical Engineering Department, Shahid Bahonar University of Kerman, Kerman, Iran

***Corresponding author email:** hamedahmadzadeh43@yahoo.com

Regular paper: Received: Jun. 13, 2021, Revised: Jan. 21, 2022, Accepted: Jan. 29, 2022, Available Online: Jan. 31, 2022, DOI: 10.52547/ijop.15.2.167

ABSTRACT— Graphene and molybdenum disulfide (MoS_2), as two of the most attractive two-dimensional (2D) materials, are used to improve the temperature and strain sensing responses of the few-mode fibers (FMFs). The temperature and strain effects are detected based on distributed optical fiber sensors equations, where the Brillouin scattering (BS) is investigated for the FMF tapered region. For this purpose, the 2D materials were assumed as cover layers on the tapered FMF to enhance its sensitivity. Graphene and MoS_2 are used as the cover layer on the FMF cladding at a distance of 10 μm from the core, and the impact of the number of material layers is investigated. By increasing the graphene layers, the temperature and strain sensitivities increase (3% and 16%, respectively) due to the rise of the inter-modal interference of the FMF. Moreover, the increasing of the MoS_2 layer number improves the temperature sensitivity by 28% but shows a lower impact on strain sensitivity (about 13%). The advantage of MoS_2 with respect to graphene originates from the imaginary part of the refractive index of graphene (assumed with chemical potential of 0.4 eV at the working wavelength of 1550 *nm*), which leads to a lower effective index of the tapered region, hence lower sensitivities. This sensitivity enhancement can improve the performance of the BS-based sensors for local detection of the parameters under-investigation in multi-parameter sensors.

KEYWORDS: Brillouin Scattering, Few-Mode Fiber, Graphene, Molybdenum Disulfide, Strain sensor, Temperature sensor.

I. INTRODUCTION

Optical fiber sensors (OFS) have been extensively studied in recent decades, due to advantages such as reliability, high sensitivity, ultra-compact low-cost fabrication [1], [2], and remote sensing capability. Thanks to modern technologies, OFSs can be utilized to measure diverse parameters including temperature, strain, pressure, and hence curvature, and so on. There are many fiber-optic technologies that can be applied to realize the sensing performance of optical fibers including fiber interferometers [3]-[6], scattering effects [7]-[9], fiber Bragg gratings, fiber coupler, and so on. Owing to the unique property of the simple implementation, various types of single-mode fibers (SMFs) are widely used in OFSs. Some instances include standard single-mode fiber (SSMF) [10], polarization-maintaining fiber (PMF) [11], single-mode photonic crystal fiber (SM-PCF) [12] or polarization-maintaining PCF (PM-PCF) [13].

Few-mode Fibers (FMFs), on the other hand, have been increasingly used in optical communication systems in recent years, owing to numerous advantages such as high transmission capacity which can overcome the limited capacity of traditional SMFs. Moreover, FMFs are used instead of SSMFs as distributed optical sensors because they confine more scattered light and have higher sensitivity and resolution [14]-[16].

[Downloaded from ijop.ir on 2026-11-16]

Distributed OFSs can determine the spatial distribution of the parameter under-investigation along the desired part of the fiber, rather than a single point sensing. They work mainly based on optical scattering phenomena such as Rayleigh, Brillouin, or Raman scattering, and can detect the variations of the temperature and strain [17].

Several different groups have so far investigated the distributed OFSs based on the stimulated Brillouin scattering (SBS) using FMFs. They have measured various parameters such as temperature, strain, pressure, and curvature using FMFs. Li *et al*. fabricated two types of FMF sensors (discrete and distributed) to achieve a unique FMF-based multi-parameter sensor in 2015 [18]. Also, Weng *et al*. experimentally measured the temperature and strain parameters simultaneously via the FMF-based distributed OFSs using Brillouin optical time-domain reflectometry (OTDR) and heterodyne detection in 2015 [19]. Another group also measured two parameters (temperature and curvature) simultaneously along an FMF by using an OTDR system, based on Brillouin and Raman effects in 2017 [20]. Multimode spectroscopy could be also applied on FMF-based sensors to decouple different parameters under investigation [21] which makes FMF sensors much more suitable for multi-parameter sensing than their SMF counterparts.

Two-dimensional (2D) materials such as graphene, phosphorene, silicene, hexagonal Boron Nitride (h-BN), and transition metal-dichalcogenides (TMDCs), have been recently highly regarded by scientists, because of their special electrical and optical properties. Among these materials, the optical response of graphene is well known and its intrinsic zero bandgap can be tuned by applying an electrostatic field or chemical doping injection [22]. Therefore, graphene is used in many devices such as optical absorbers [23], filters [24], [25], optical sensors [26], and modulators [27].

On the other hand, TMDCs such as molybdenum disulfide (MoS_2), molybdenum diselenide ($MoSe_2$), tungsten disulfide (WS_2), and tungsten diselenide (WSe_2) have specific direct band gaps similar to semiconductors [28]. A widely used TMDC, i.e. MoS_2, is more attractive in photovoltaic devices [29], transistors [30], and optical sensors [31] due to its high refractive index. This property makes it particularly appropriate in sensor applications.

Here we investigate the effects of graphene and MoS_2 on the sensing of temperature and strain in an FMF. These two 2D materials are used as the cover of the tapered FMF with a distance of 10 μm from the core. Their unique optical properties improve the sensitivity of the FMF sensor regarding temperature and strain. Before we discuss these effects, the theoretical assumptions of the FMF sensors – working based on Brillouin Scattering (BS) – are discussed in more detail in section 2. Discussions on the effects of applying graphene and MoS_2 on the FMF cladding (hence its modes and sensitivities) are brought in section 3 and it is shown that the MoS_2 is much more effective on the temperature and strain sensing than graphene, for multi-parameter sensing. There is also a comparison between the bare sensors based on FMF that do not use the 2D materials with the sensors covered by MoS_2/graphene. The results are concluded finally, in section 4. All the simulations are performed using the finite element method (FEM) employing the COMSOL Multiphysics package; first, the indices are calculated, and then they are used to calculate BS. The two-dimensional materials also are modeled using a transition boundary condition, in which a discontinuity is applied to the electric fields on different sides of the boundary, based on material thickness and its optical properties.

II. THEORETICAL ASPECT

We use the distributed OFS formulation to detect the temperature and strain variations applied to the fiber. This section briefly introduces the basics of these distributed OFSs. The distributed OFS is expected to demonstrate temperature, strain, and vibration information at any point along the fiber using light scattering. The phenomenon of light scattering

[Downloaded from ijop.ir on 2026-11-16]

may occur due to various causes such as non-uniformity of material density, change in the material refractive index, and other similar variations that change the optical properties of the fiber. Among different scattering phenomena that may occur in any fiber [32], BS is surveyed here to demonstrate thermal or mechanical changes within the fiber. BS, which is an inelastic scattering, is used because it originates from changes in the material refractive index due to the propagation of the acoustic waves in the optical fiber. In other words, variations of the temperature, strain, or pressure to one part of the fiber initiate some acoustic waves, and the BS is observed.

Since FMFs support more than one mode, the BS can be observed not only in one spatial mode but also between different spatial mode pairs [33], called intra- and inter-modal BSs. This paper focuses on inter-modal BS, and the idea behind its generation in an FMF, where the associated formulae are brought in the following. When the (pump) light is propagating in a long FMF with the wavelength λ and mode i, a portion of the light will be backscattered because of the interaction between light photons and acoustic phonons. The phenomenon can occur spontaneously which is known as spontaneous BS, in which acoustic phonons stem from thermal variations. By increasing the optical power, the acoustic phonons, which are mainly generated from the optical field, cause stimulated BS. The light is scattered as the Stokes waves with a lower frequency (equal to the acoustic wave frequency), owing to the moving grating originating from the acoustic wave which is called the Doppler shift. The dependency of the scattered light on the acoustic velocity is given by the following equation [34]:

$$v_B = \frac{2n_i V_a}{\lambda}\sin\left(\frac{\theta}{2}\right) \tag{1}$$

where v_B, n_i, V_a, and θ are respectively, the Brillouin frequency shift (BFS), the effective refractive index (ERI) of i^{th} mode, the effective velocity of the acoustic wave, and the angle between the pump and the Stokes fields. Within an optical fiber, for the forward direction (θ=0) BFS vanishes (v_B=0), while for the backward direction ($\theta=\pi$) it is maximum and can be described as $v_B=2n_iV_a/\lambda$.

Since the acoustic velocity in a silica fiber is dependent on the temperature and strain, therefore for the inter-modal SBS effect, the temperature and strain dependency of the BFS can be obtained by partial derivatives of Eq. (1) for ($\theta=\pi$):

$$\frac{dv_B}{dT} = \frac{2}{\lambda}\left(V_a\frac{dn_i}{dT} + n_i\frac{dV_a}{dT}\right) \approx \frac{2n_i}{\lambda}\frac{dV_a}{dT} \tag{2}$$

$$\frac{dv_B}{d\varepsilon} = \frac{2}{\lambda}\left(V_a\frac{dn_i}{d\varepsilon} + n_i\frac{dV_a}{d\varepsilon}\right) \approx \frac{2n_i}{\lambda}\frac{dV_a}{d\varepsilon} \tag{3}$$

In Eqs. (2) and (3), changes in the refractive index concerning the temperature and strain are negligible and can be ignored [18]. It is also noteworthy that the BFS is extremely dependent on the refractive index, but the refractive index itself plays not an important role here, and the ERI is the important factor that will be shown in the following. However, the BFS changes through the velocity of the acoustic wave. This means that by changing an external parameter such as temperature or strain, the BFS changes via the acoustic wave velocity. This concept is evident in Eq. (4) [35] where E is Young's modulus, κ is the Poisson's ratio and ρ is the density:

$$V_a = \sqrt{\frac{E(1-\kappa)}{(1+\kappa)(1-2\kappa)\rho}} \tag{4}$$

Each of these parameters is directly related to the temperature of the device (the relationships are given in [36]). Therefore, the acoustic wave velocity is indirectly related to the temperature. Nonetheless, it can be easily shown that [35]:

$$\frac{1}{V_a}\frac{\partial V_a}{\partial\varepsilon} = \frac{1}{v_B}\left(\frac{\partial V_a}{\partial E}\frac{\partial E}{\partial\varepsilon} + \frac{\partial V_a}{\partial\kappa}\frac{\partial\kappa}{\partial\varepsilon} + \frac{\partial V_a}{\partial\rho}\frac{\partial\rho}{\partial\varepsilon}\right)$$
$$= \underbrace{\frac{1}{2E}\frac{\partial E}{\partial\varepsilon}}_{\delta E} + \underbrace{\frac{\kappa(2-\kappa)}{(1-\kappa^2)(1-2\kappa)}\frac{\partial\kappa}{\partial\varepsilon}}_{\delta\kappa} - \underbrace{\frac{1}{2\rho}\frac{\partial\rho}{\partial\varepsilon}}_{\delta\rho} \tag{5}$$

[Downloaded from ijop.ir on 2026-11-16]

Thus, the deviations of these three parameters, i.e. variations of Young's modulus (δE), Poisson's ratio ($\delta\kappa$) and the density ($\delta\rho$), can be expressed as a function of the strain variations. By calculating each of these parameters, the dependency of acoustic wave velocity can be calculated on the strain.

Studying the equations of the SBS phenomenon, one can obviously observe the direct dependency of the BFS to V_a. The latter is basically a function of the temperature (T) and density (ρ). Hence, variations of these quantities can be detected by measuring the BFS. Because of the elastic property of silica, little amounts of strain variations change the volume and thus the density of the fiber and the sensing can be performed.

III. Results and Discussion

A. *BSF Shift of the Bare FMF (without 2D Material Cover)*

The optical fibers parameters used in this paper are given in Table 1, where it has a step-index profile between core and cladding. For the FMF, 6 linearly polarized (LP) spatial modes, namely LP_{01}, LP_{11a}, LP_{11b}, $LP2_{1a}$, $LP2_{1b}$, and LP_{02}, are supported at the working wavelength of 1550 *nm*. The field distribution profiles for these modes are shown in Fig. 1, where the boundary between the core and cladding is marked with a black solid circle.

Before examining the effects of 2D materials on the temperature and strain sensing in FMF, the SMF and FMF were compared, without using 2D materials. Having the equation of acoustic velocity (Eq. (4)) as well as the refractive index of each of the propagating modes in both SMF and FMF, the temperature and strain dependencies of the BFS are obtained, according to Eqs. (2) and (3), respectively (please see Fig. 2).

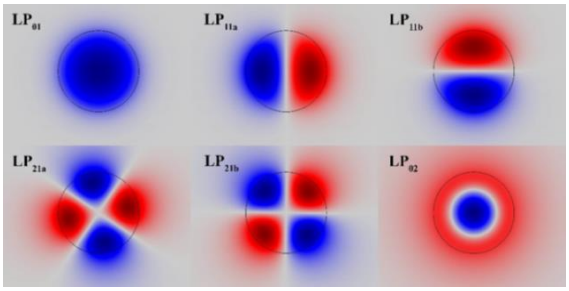

Fig. 1. LP mode field distribution for FMF. The black circle shows the boundary between core and cladding.

The slopes of the curves in Figs. 2(a) and 2(b) show the sensitivity of each mode in SMF and FMF in the temperature range of -40 to 100 °C. Although lower-order modes of the FMF (i.e. LP_{01} and LP_{11}) have higher temperature sensitivities (1.035 and 1.016 MHz/°C) than the SMF (1.001 MHz/°C), higher-order modes (LP_{02} and LP_{21}) in FMF have lower sensitivity (0.990 and 0.989) than SMF (1.001). Figures 2 (c) and (d) show the BFS associated with different applied stains (ranging from 0 to 8000 $\mu\varepsilon$) for the SMF and FMF modes. Here, the sensitivity, i.e. the slope of the curves is 0.0565, 0.0555, 0.0545, 0.0540, and 0.0550 (MHz/$\mu\varepsilon$) for LP_{01}, LP_{11}, LP_{02}, LP_{21}, and the SMF, respectively. Just similar to the temperature sensitivity, the two higher-order modes show lower strain sensitivity than the SMF fiber mode.

Table **1** SMF and FMF Parameters

Parameters of SMF	**Value**	**Unit**	**Parameters of FMF**	**Value**	**Unit**
Core Diameter SMF	8	µm	Core Diameter FMF	14.4	µm
Cladding Diameter SMF	125	µm	Cladding Diameter FMF	125	µm
Core Refractive Index	1.4519	-	Core Refractive Index	1.4519	-
Cladding Refractive Index	1.4440	-	Cladding Refractive Index	1.4440	-
Effective Refractive Index of LP_{01}	1.4441	-	Effective Refractive Index of LP_{01}	1.4505	-
-	-	-	Effective Refractive Index of LP_{11}	1.4481	-
-	-	-	Effective Refractive Index of LP_{21}	1.4453	-
-	-	-	Effective Refractive Index of LP_{02}	1.4446	-

[Downloaded from ijop.ir on 2026-11-16]

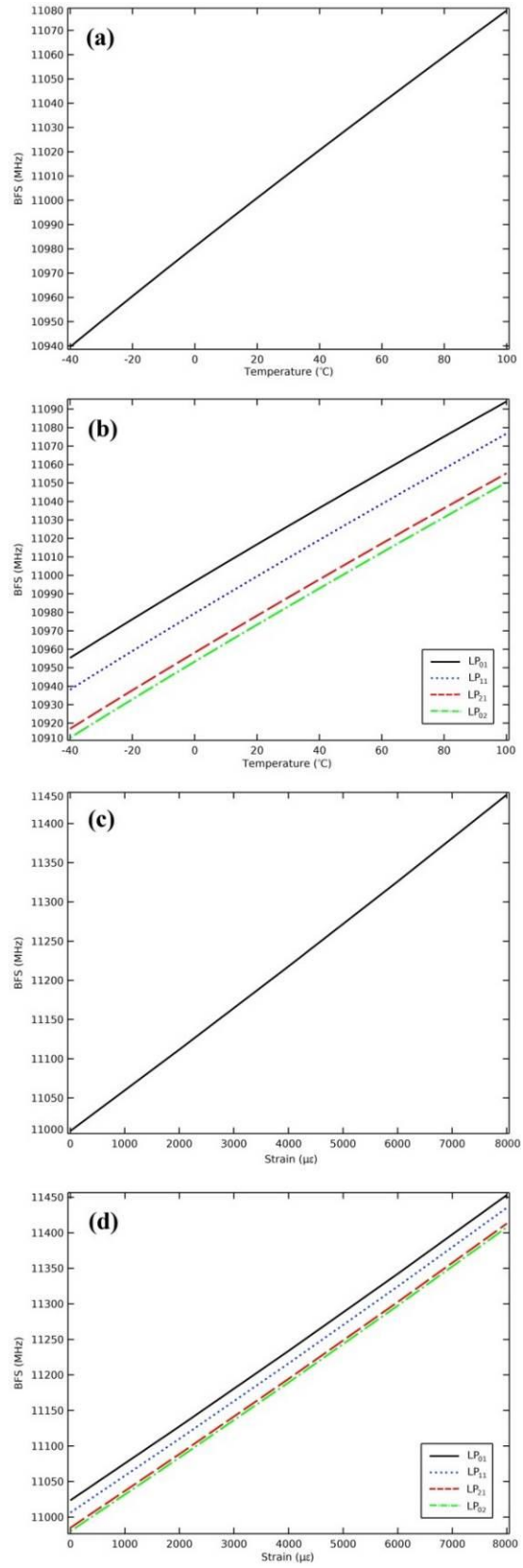

Fig. 2. BFS vs. temperature for (a) SMF and (b) FMF and strain for (c) SMF and (d) FMF at 1550 *nm*.

The higher sensitivity of the SMF in comparison to higher-order modes of the FMF, for both temperature and strain, originates from the higher confinement of the light within the core, since it is obvious from Eqs. 2 and 3, the sensitivity is linearly related to the ERI of the modes. For higher-order modes (LP_{02} and LP_{21}), the ERIs (1.4453 and 1.4446) are lower than the ERI of the SMF (1.4479). For lower modes, the higher ERIs (1.4505 and 1.4481 for LP_{01} and LP_{11}, respectively) justify the higher sensitivity. The temperature and strain sensitivity values for each of the modes in the SMF and FMF are more discussed in Table 3, at the end of section 3.

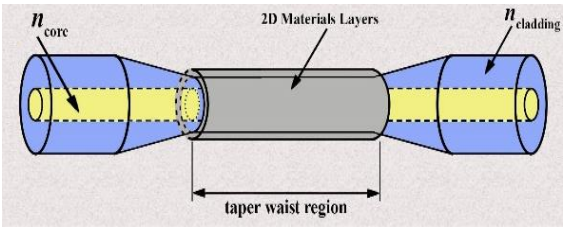

Fig. 3. The proposed FMF for temperature and strain sensing.

B. *BSF Shift of the Tapered FMF with 2D Material Cover*

If we want to use the 2D material as the cover on the FMF fiber, the fiber must be etched and a taper FMF should be formed first. This leads to enough interaction of the modes within the core and the 2D material, which is not possible for a standard fiber with typical cladding. In a standard fiber, the evanescent electric field is adjacent to the fiber core, and cannot reach the external ambient. For a tapered fiber, on the other hand, the evanescent field of the fiber can reach the external boundaries; hence the 2D materials, which may be deposited on the fiber [37], [38], can contribute to the sensing phenomenon. Figure 3 shows a schematic of the tapered FMF, where a simple FMF is assumed to be manipulated in such a way that a waist region is formed with the cladding narrowed to 10 μm. Stretching the waist region under different conditions could lead to various cladding or core diameters [39], but it may also change the core diameter. Here, we assumed a condition in which the core diameter doesn't experience any meaningful change, which can be formed using chemical etching of the cladding, e.g. using HF solution [40]. Therefore, the sensing region includes two tapered regions and one waist region where the

[Downloaded from ijop.ir on 2026-11-16]

2D material can be formed on the cladding of the waste region with the fixed cladding of 10 μm.

To investigate the effects of the covering 2D material in the tapered fiber, we first investigate the impact of the graphene layer(s) on the temperature and strain parameters in the FMF. To simulate graphene, boundary conditions were used with the surface conductivity of the graphene (σ_g). For a single layer of graphene, σ_g is calculated through the well-known Kubo formula, where analytic formulae were used for both the inter-band and intra-band conductivity contributions [22].

$$\sigma_g = \sigma_{intra} + \sigma_{inter} \tag{6}$$

$$\sigma_{intra} = i\frac{2e^2 k_B T}{\pi\hbar^2\left(\omega + i\tau^{-1}\right)}\ln\left(2\cosh\left(\frac{\mu_c}{2k_B T}\right)\right), \tag{7}$$

$$\sigma_{inter} = \frac{\pi e^2}{4h}\left(\tanh\frac{\hbar\omega + 2\mu_c}{4k_B T} + \tanh\frac{\hbar\omega - 2\mu_c}{4k_B T}\right) + i\frac{e^2}{2h}\left(\frac{4\mu_c}{\hbar\omega} + \ln\sqrt{\left|\frac{\hbar\omega - 2\mu_c}{\hbar\omega + 2\mu_c}\right|}\right). \tag{8}$$

Intrinsically, Graphene has a zero bandgap structure that can be manipulated by various methods such as applying electrostatic field or chemical doping injection. These methods can change the chemical potential of graphene (μ_c), which results in the tuning of its bandgap as well, and consequently, its electronic properties can be adjusted. In this paper, for all of the simulations μ_c is assumed to be 0.4 eV, which provides a high refractive index for graphene. In other words, for the 1550 *nm* optical window (when μ_c=0.4 eV) the real and imaginary parts of the refractive index of graphene (n_g) have a high positive contribution (5.6163+0.74178*i*), which influence the refractive indices of the guided modes in the underlying FMF.

In such a tapered fiber with graphene cover, the light is not confined within the core with total internal reflection and tends to be coupled into the covered 2D material. Moreover, in these circumstances, relatively high losses may occur because of the high imaginary part of n_g. Besides the higher sensitivity, the advantage of the proposed tapered FMF with graphene cover is its ultra-fast response to temperature variations, as the temperature is measured on the outer surface of the fiber, instead of the core, due to the movement of the mode from the core into the cover. This is also true for the case of MoS_2 which is discussed later. Figure 4 shows the ERIs of the modes for the FMF with/without 2D materials. ERIs turn to complex values when 2D materials are applied at the covering of the tapered FMF. However, the higher real part of the ERIs promises higher sensitivities, as well as transmission losses. Moreover, for higher propagating mode orders in the FMF lower BFS is observed, because of the lower refractive indices of these modes.

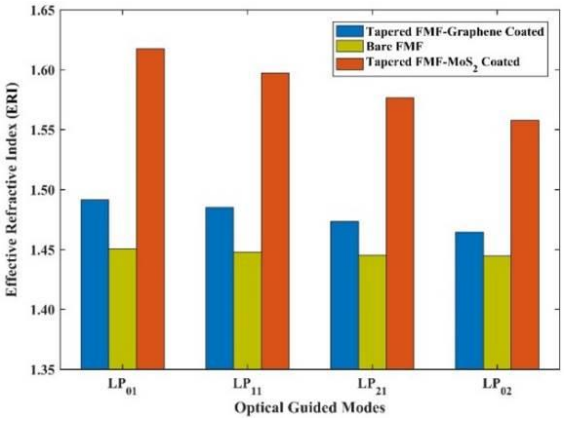

Fig. 4. The real part of the guided modes ERIs for the FMF with/without 2D materials.

Figures 5(a) and (b) show the relationship between the BFS with the temperature and strain, respectively, for different modes of the FMF. Here, 10-layer graphene is employed, because the increasing of graphene layers results in higher ERI, which is surveyed in the next figure (thickness of single-layer graphene is assumed to be 0.34 *nm*). For 10 layers, the materials can be assumed as 2D materials (compared to the fiber diameter) and their properties are still valid [41], [42]. As a result, the guided modes inside the FMF core, affected by the graphene layers, couple into the cover, and their refractive indices also change. Increasing the ERIs leads to smoothly higher sensitivities for graphene-coated tapered FMF with respect to SMF or FMF without the coating.

[Downloaded from ijop.ir on 2026-11-16]

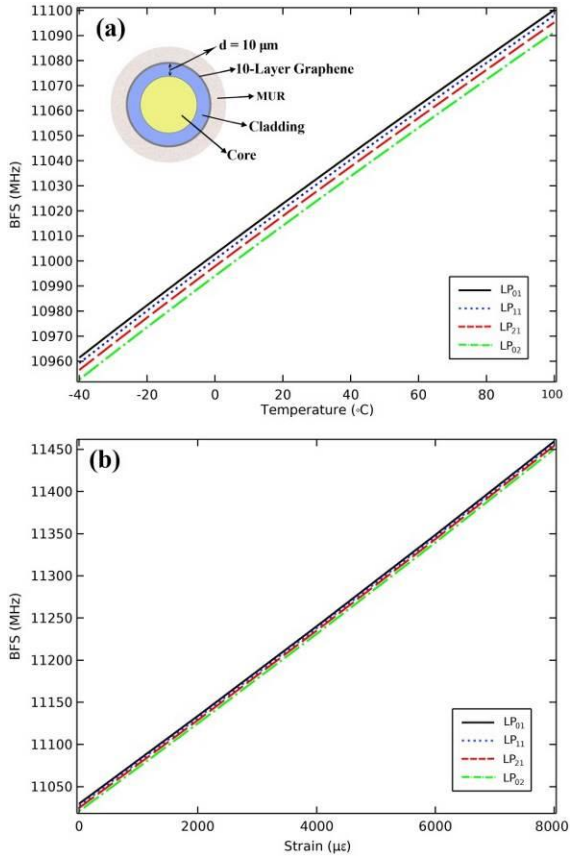

Fig. 5. Relationship between BFS and (a) temperature and (b) strain at the wavelength of 1550 *nm* for 10-layer graphene.

The effect of the number of the graphene layers (N_g) on the BFS is shown in Fig. 6. The simulations have been run at the temperature of 100°C and the strain of 8000 $\mu\varepsilon$ (parts (a) and (b) of the figure, respectively). It can be seen from Fig. 6 that when N_g increases, the resolution between the 4 modes decreases. Lower-order modes are less influenced by N_g because they are more confined within the core, while higher-order modes show much more variation with respect to N_g multiplicity. However, the increment of the sensitivity concerning N_g multiplicity has similar trends. It must be noted that for N_g > 10, inter-modal interference will be occurred, which is not suitable for multimode spectroscopy and must be avoided. In the cases with inter-modal interference, the ERI of the modes merge and some modes may combine to each other. Therefore, 10 layers are chosen which enhance the sensitivity for higher modes, while the interference is still prevented. Moreover, the multimode sensing can be used to enhance the selectivity between parameters under-investigation [21].

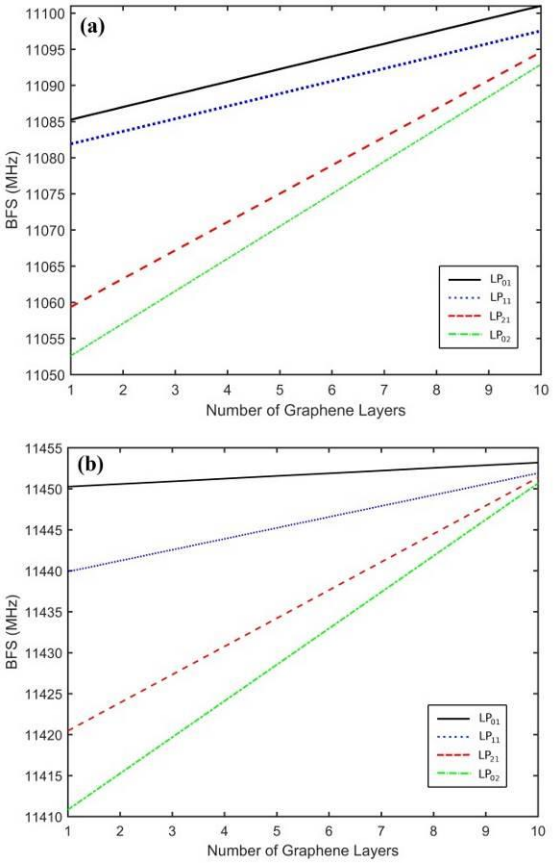

Fig. 6. Investigation of the effect of different layers of graphene on the BFS as functions of (a) temperature (at 100 °C), and (b) strain (for 8000 $\mu\varepsilon$), for different propagating modes.

In the second part of Section 3.2, the effects of the MoS_2, as the FMF coating, are studied. MoS_2 is a member of TMDCs, which has special electronic and optical properties. MoS_2 is a graphene-like material with a 2D honeycomb structured lattice, consisting of monoatomic molybdenum (M) layer sandwiched between two monoatomic sulfide (S) layers [39]. In contrast with intrinsic graphene, the band structure of MoS_2 has a bandgap, and also its refractive index is very high (4.25). In the present work, the Lorenz model is used to obtain the MoS_2 relative permittivity [43]:

$$\varepsilon_{MoS_2} = \varepsilon_\infty + \sum_{j=1}^{5} \frac{a_j}{\omega_j^2 - \omega^2 - i\omega b_j} \quad (9)$$

here, ε_∞ is 2.2 and a_j, ω_j, and b_j values are adopted as Table 2.

[Downloaded from ijop.ir on 2026-11-16]

Table **2** Coefficients a_j, b_j, and ω_j correspond to the Lorentz model for MoS_2

j	a_j [eV^2]	b_j [eV]	ω_j [eV]
1	0.950	0.072	1.865
2	2.000	0.120	2.008
3	36.54	0.380	2.868
4	11.00	1.000	2.275
5	100.0	0.400	3.745

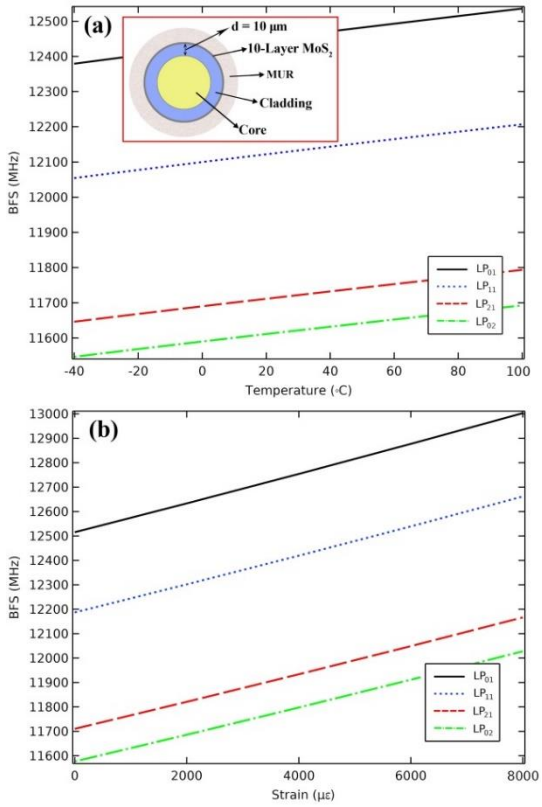

Fig. 7. Relationship between BFS and (a) temperature and (b) strain at the wavelength of 1550 *nm* for 10-layer MoS_2.

The characteristic curves of the BFS for temperature and strain variations are shown in Figs. 7(a) and (b), for the case where MoS_2 has 10 layers. Just similar to the case of graphene coating, MoS_2 layers are considered to be coated on the FMF cladding at a distance of 10 μm from the core (shown in the inset of Fig. 7(a)). When 10-layers MoS_2 is used, the MoS_2 refractive index impact increases tenfold. Therefore, the guided modes inside the FMF core are strongly affected by the MoS_2 layers, and their ERIs change accordingly (see Fig. 4). Thus, the curves experience a large increase in the BFS. The existence of MoS_2 on the cover of the cladding has a direct effect on the BFS, just like the graphene layer. But unlike the graphene, the MoS_2 refractive index has a little imaginary part in wavelength of 1550 *nm*, and the real part is still large (4.25 - 0.096i). Therefore, it strongly impacts the propagating modes of the FMF, and their sensitivity increases much more than graphene (brought in Table 3).

The effects of different numbers of MoS_2 layers (N_{MoS2}) on the BFS are shown in Figs. 8 for the temperature of 100 °C and strain of 8000 $\mu\varepsilon$. As shown in Fig. 8, increasing the number of MoS_2 layers, unlike the case for graphene, causes the resolution between the modes to increase. This is because, with the increase of N_{MoS2}, the propagating modes in the FMF are more affected by its real part of the refractive index, since its imaginary part is low.

To compare graphene and MoS_2, One can conclude that in this wavelength (1550 *nm*), graphene with 0.4 eV chemical potential works as a weak metal, though it shows some losses as well. Nevertheless, the metallic behavior of graphene lets the higher-order modes with lower ERIs contribute more, as their confinements are weaker and they can enhance the electric field on the graphene surface more than lower-order modes. Because of this field enhancement, these higher-order modes are more susceptible to the changes of the material mechanical parameters (see Eq. (5)). Therefore, their sensitivity increases. For the case of MoS_2, the metallic behavior of the material is insignificant (since the imaginary part of its refractive index is negligible as well). Thus, the modes only are affected by the real part of the MoS_2 refractive index and the sensitivity of higher-order modes changes less than lower ones. As a result, the multiplicity of MoS_2 layers increases the resolution of the modes, and thus the temperature and strain sensitivity. Comparing Figs. 6 and 8, one can conclude that increasing the graphene layers increases the inter-modal interference in the FMF, but unlike graphene, the multiplicity of MoS_2 layers increases the inter-modal resolution. Besides the higher increment of the sensitivity for tapered FMF fiber covered with MoS_2, for both temperature and strain, mode interference is another factor that shows the advantages of MoS_2 with respect to graphene. Another

[Downloaded from ijop.ir on 2026-11-16]

important aspect of applying 2D materials is the increase of the slope of the curves for lower order modes, suggesting higher sensitivities.

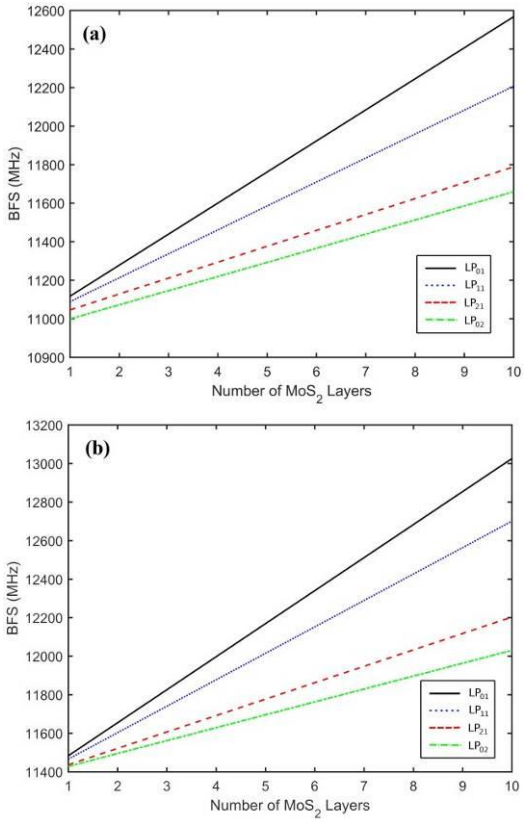

Fig. 8. Investigation of the effect of different layers MoS_2 on the BFS as a function of temperature and strain for 4 modes at (a) 100 ℃ and (b) 8000 $\mu\varepsilon$.

To clear the perception of the effect of graphene and MoS2 layers on the temperature and strain sensitivity of modes, the values related to temperature and strain sensitivity for propagating modes in the FMF are given in Table 3. These values are compared with [18] and our results in section 3.1 (for SMF and bare FMF).

Adding graphene and MoS_2 layers increase both the temperature and strain sensitivities for the propagating modes. In comparison with [18], our results show higher sensitivities for both the temperature and strain. However, using 10 graphene layers did not significantly increase the temperature sensitivity (only 3% relative to bare FMF), but 10 MoS_2 layers increase the temperature sensitivity by about 28%. The strain sensitivity values for 10-layer graphene and MoS_2 increase by 16% and 13% relative to the bare FMF, respectively. Unlike temperature sensitivity, graphene has a greater effect on strain sensitivity than MoS_2. Utilizing different modes of the FMF when multiple parameters are sensed simultaneously could lead to a decoupling of the parameters under investigation, which can be emerged using multi-mode spectroscopy. This, besides the enhancement achieved by the proposed 2D materials covered on the tapered fiber, can improve the performance of the BS-based multi-parameter sensors.

Table **3** Comparison of temperature and strain sensitivity of modes in this work with those of [18].

	Structure		**Mode**			
			LP_{01}	**LP_{11}**	**LP_{21}**	**LP_{02}**
Temperature sensitivity (MHz/℃)	Bare Fibers	SMF	1.001	-	-	-
		Bare FMF	1.035	1.016	0.990	0.989
		[18]	1.01693	0.99099	-	-
	2D Coated Tapered Fibers	Graphene	1.07857	1.06428	1.05021	1.03571
		MoS_2	1.42857	1.21428	1.07142	0.96428
Strain sensitivity (MHz/$\mu\varepsilon$)	Bare Fibers	SMF	0.0550	-	-	-
		Bare FMF	0.0565	0.0555	0.0545	0.0540
		[18]	0.05924	0.04872	-	-
	2D Coated Tapered Fibers	Graphene	0.07125	0.07102	0.07062	0.07010
		MoS_2	0.06875	0.06450	0.06025	0.05750

[Downloaded from ijop.ir on 2026-11-16]

IV. CONCLUSION

In this paper, the effect of different 2D materials on the temperature and strain sensitivity in an FMF-based sensor was investigated and the improvement of the BS-based sensor for multi-parameter sensors was attained. Graphene and molybdenum disulfide (MoS_2), are considered such that they are formed on the FMF cladding at a distance of 10 micrometers from the FMF core as a cover on the tapered FMF. The simulation results show that 10 layers of graphene increase the temperature and strain sensitivity by 3% and 16%, respectively. On the other hand, the use of 10 layers of MoS_2 increases temperature and strain sensitivities by 28% and 13%, respectively. The effects of a multiplicity of layers of these 2D materials are also investigated and it is observed that increasing the graphene layers increases the inter-modal interference in the FMF, and graphene should be used with low layers only. But unlike graphene, the multiplicity of MoS_2 layers reduces the inter-modal interference in the FMF.

Finally, with the usage of the 2D material (either graphene or MoS2) as the covering layer on the cladding of the tapered FMF-based sensors, it is possible to build a multi-parameter sensor that could be used in multimode spectroscopy.

REFERENCES

[1] B. Lee, "Review of the present status of optical fiber sensors," Opt. Fiber Technol. Vol. 9, pp. 57-79, 2003.

[2] G. Rajan, *Optical fiber sensors: advanced techniques and applications*, CRC press, 2017.

[3] P. Orr and P. Niewczas, "High-speed, solid state, interferometric interrogator and multiplexer for fiber Bragg grating sensors," J. Lightwave Technol. Vol. 29, pp. 3387-3392, 2011.

[4] S.-C. Her and C.-M. Yang, "Dynamic strain measured by Mach-Zehnder interferometric optical fiber sensors," Sensors, Vol. 12, pp. 3314-3326, 2012.

[5] X. Li, Y. Shao, Y. Yu, Y. Zhang, and S. Wei, "A highly sensitive fiber-optic Fabry–Perot interferometer based on internal reflection mirrors for refractive index measurement," Sensors, vol. 16, pp. 794 (1-12), 2016.

[6] H. Moradi, P. Parvin, F. Shahi, and A. Ojaghloo, "Fiber optic Fabry–Pérot acoustic sensor using PVC and GO diaphragms," OSA Continuum, Vol. 3, pp. 943-951, 2020.

[7] X. Bao and L. Chen, "Recent progress in Brillouin scattering based fiber sensors," Sensors, Vol. 11, pp. 4152-4187, 2011.

[8] P. Lu, N. Lalam, M. Badar, B. Liu, B.T. Chorpening, M.P. Buric, and P.R. Ohodnicki, "Distributed optical fiber sensing: Review and perspective," Appl. Phys. Rev. Vol. 6, pp. 041302 (1-35), 2019.

[9] L. Palmieri and L. Schenato, "Distributed optical fiber sensing based on Rayleigh scattering," The Open Opt. J. Vol. 7, pp. 104-127, 2013.

[10] T. Feng, J. Zhou, Y. Shang, X. Chen, and X.S. Yao, "Distributed transverse-force sensing along a single-mode fiber using polarization-analyzing OFDR," Opt. Express, Vol. 28, pp. 31253-31271, 2020.

[11] Y. Liu, B. Liu, X. Feng, W. Zhang, G. Zhou, S. Yuan, G. Kai, and X. Dong, "High-birefringence fiber loop mirrors and their applications as sensors," Appl. Opt. Vol. 44, pp. 2382-2390, 2005.

[12] J. Villatoro, V. Finazzi, V.P. Minkovich, V. Pruneri, and G. Badenes, "Temperature-insensitive photonic crystal fiber interferometer for absolute strain sensing," Appl. Phys. Lett. Vol. 91, pp. 091109 (1-3), 2007.

[13] X. Dong, H. Tam, and P. Shum, "Temperature-insensitive strain sensor with polarization-maintaining photonic crystal fiber based Sagnac interferometer," Appl. Phys. Lett. Vol. 90, pp. 151113 (1-3), 2007.

[14] R.W. Tkach, "Scaling optical communications for the next decade and beyond," Bell Labs Technical J. Vol. 14, pp. 3-9, 2010.

[15] K.-i. Kitayama and N.-P. Diamantopoulos, "Few-mode optical fibers: Original motivation and recent progress," IEEE Commun. Mag. Vol. 55, pp. 163-169, 2017.

[16] S. Randel, R. Ryf, A. Sierra, P.J. Winzer, A.H. Gnauck, C.A. Bolle, R.-J. Essiambre, D.W.

[Downloaded from ijop.ir on 2026-11-16]

Peckham, A. McCurdy, and R. Lingle, "6× 56-Gb/s mode-division multiplexed transmission over 33-km few-mode fiber enabled by 6× 6 MIMO equalization," Opt. Express, Vol. 19, pp. 16697-16707, 2011.

[17] A.H. Hartog, *An introduction to distributed optical fibre sensors*, CRC press, 2017.

[18] A. Li, Y. Wang, Q. Hu, and W. Shieh, "Few-mode fiber based optical sensors," Opt. Express, Vol. 23, pp. 1139-1150, 2015.

[19] Y. Weng, E. Ip, Z. Pan, and T. Wang, "Single-end simultaneous temperature and strain sensing techniques based on Brillouin optical time domain reflectometry in few-mode fibers," Opt. Express, Vol. 23, pp. 9024-9039, 2015.

[20] H. Wu, M. Tang, M. Wang, C. Zhao, Z. Zhao, R. Wang, R. Liao, S. Fu, C. Yang, and W. Tong, "Few-mode optical fiber based simultaneously distributed curvature and temperature sensing," Opt. Express, Vol. 25, pp. 12722-12732, 2017.

[21] F. Bahrami, J.S. Aitchison, and M. Mojahedi, "Multimode Spectroscopy in Optical Biosensors," Biomed. Opt. Sensors, pp. 57-79, 2020.

[22] M. Maleki, M. Mehran, and A. Mokhtari, "Design of a near-infrared plasmonic gas sensor based on graphene nanogratings," J. Opt. Soc. Am. B, Vol. 37, pp. 3478-3486, 2020.

[23] D. Wu, M. Wang, H. Feng, Z. Xu, Y. Liu, F. Xia, K. Zhang, W. Kong, L. Dong, and M. Yun, "Independently tunable perfect absorber based on the plasmonic properties in double-layer graphene," Carbon, Vol. 155, pp. 618-623, 2019.

[24] M. Janfaza, M.A. Mansouri-Birjandi, and A. Tavousi, "Proposal for a graphene nanoribbon assisted mid-infrared band-stop/band-pass filter based on bragg gratings," Opt. Commun. Vol. 440, pp. 75-82, 2019.

[25] M. Janfaza, M.A. Mansouri-Birjandi, and A. Tavousi, "Tunable plasmonic band-pass filter based on Fabry–Perot graphene nanoribbons," Appl. Phys. B, Vol. 123, pp. 262 (1-9), 2017.

[26] Z. Zhang, J. Yang, X. He, J. Zhang, J. Huang, D. Chen, and Y. Han, "Plasmonic refractive index sensor with high figure of merit based on concentric-rings resonator," Sensors, Vol. 18, pp. 116 (1-14), 2018.

[27] F. Sun, L. Xia, C. Nie, C. Qiu, L. Tang, J. Shen, T. Sun, L. Yu, P. Wu, S. Yin, S. Yan, and C. Du "An all-optical modulator based on a graphene–plasmonic slot waveguide at 1550 nm," Appl. Phys. Express, Vol. 12, pp. 042009 (1-10), 2019.

[28] Q.H. Wang, K. Kalantar-Zadeh, A. Kis, J.N. Coleman, and M.S. Strano, "Electronics and optoelectronics of two-dimensional transition metal dichalcogenides," Nature Nanotechnol. Vol. 7, pp. 699-712, 2012.

[29] M. Bernardi, M. Palummo, and J.C. Grossman, "Extraordinary sunlight absorption and one nanometer thick photovoltaics using two-dimensional monolayer materials," Nano Lett. Vol. 13, pp. 3664-3670, 2013.

[30] D.J. Late, B. Liu, H.R. Matte, V.P. Dravid, and C. Rao, "Hysteresis in single-layer MoS field effect transistors," ACS Nano, Vol. 6, pp. 5635-5641, 2012.

[31] Z. Ashkavand, E. Sadeghi, R. Parvizi, and M. Zare, "Developed Low-Temperature Anionic 2H-MoS_2/Au Sensing Layer Coated Optical Fiber Gas Sensor," ACS Appl. Mater. Interfaces, Vol. 12, pp. 34283-34296, 2020.

[32] X. Bao and L. Chen, "Recent progress in distributed fiber optic sensors," Sensors, Vol. 12, pp. 8601-8639, 2012.

[33] K.Y. Song, Y.H. Kim, and B.Y. Kim, "Intermodal stimulated Brillouin scattering in two-mode fibers," Opt. Lett. Vol. 38, pp. 1805-1807, 2013.

[34] G.P. Agrawal, *Nonlinear fiber optics, Nonlinear Science at the Dawn of the 21st Century*, Springer, pp. 195-211, 2000.

[35] S.F. Mafang, "Brillouin echoes for advanced distributed sensing in optical fibres," École Polytechnique Fédérale De Lausanne, doctoral thesis, 2011.

[36] J.M. Coelho, M. Nespereira, M. Abreu, and J. Rebordão, "3D finite element model for writing long-period fiber gratings by CO2 laser radiation," Sensors, Vol. 13, pp. 10333-10347, 2013.

[37] R. Khazaeinezhad, SH. Kassani,T. Nazari, H. Jeong, J. Kim, K. Choi, J.U. Lee, J.H. Kim, H. Cheong, D.I. Yeom, and K. Oh, "Saturable optical absorption in MoS_2 nano-sheet optically deposited on the optical fiber facet," Opt. Commun. Vol. 335, pp. 224-230, 2015.

[Downloaded from ijop.ir on 2026-11-16]

[38] A. Petcu-Colan, M. Frawley, and S.N. Chormaic, "Tapered few-mode fibers: mode evolution during fabrication and adiabaticity," Journal of Nonlinear Optical Physics & Materials, Vol. 20, pp. 293-307, 2011.

[39] M. Samadi, N. Sarikhani, M. Zirak, H. Zhang, H.-L. Zhang, and A.Z. Moshfegh, "Group 6 transition metal dichalcogenide nanomaterials: synthesis, applications and future perspectives," Nanoscale Horiz. Vol. 3, pp. 90-204, 2018.

[40] H.Z. Yang, M.M. Ali, M.R. Islam, K.-S. Lim, D.S. Gunawardena, and H. Ahmad, "Cladless few mode fiber grating sensor for simultaneous refractive index and temperature measurement," Sensors and Actuators A: Physical, Vol. 228, pp. 62-68, 2015.

[41] S. Sridhar, S. Sebastian, A.K. Sood, and S. Asokan, "A Study on MoS_2 Nanolayer Coated Etched Fiber Bragg Grating Strain Sensor," IEEE Sensors J. Vol. 21, pp. 9171-9178, 2021.

[42] C. Li, X. Peng, C. Wang, S. Cao, and H. Zhang, "Few-layer MOS2-deposited flexible side-polished fiber Bragg grating bending sensor for pulse detection," IEEE 19th International Conference on Solid-State Sensors, Actuators and Microsystems (TRANSDUCERS), pp. 2007-2010, 2017.

[43] N. Ansari and F. Ghorbani, "Light absorption optimization in two-dimensional transition metal dichalcogenide van der Waals heterostructures," J. Opt. Soc. Am. B, Vol. 35, pp. 1179-1185, 2018.

Morteza Janfaza received the B.S., M.S., and Ph.D. degrees in Electrical Engineering from the University of Sistan and Baluchestan, Zahedan, Iran, in 2011, 2013, and 2019, respectively. His current research interests include graphene, nano-optics, plasmonics, surface plasmon polaritons, and photonic crystals.

Hamed Moradi received his Ph.D. in Physics from the University of Isfahan in 2019. He is currently working as a postdoctoral researcher at the Amir Kabir University of Technology. His field of activity is fiber optic sensors and semiconductor optics.

Morteza Maleki received the A.Sc. degree from the Shiraz University, Shiraz, Iran, in 2003, the B.Sc. degree from Sadjad University of Technology, Mashhad, Iran, in 2008, and the M.Sc. degree from the University of Sistan and Baluchestan, Zahedan, Iran, in 2014, all in Electronics Engineering. He is currently pursuing his study towards Ph.D. at the Electrical Engineering Department, Shahid Bahonar University of Kerman, Kerman, Iran. His research interests include optoelectronic devices, nanoelectronics, plasmonics, 2D materials, and sensors.

[Downloaded from ijop.ir on 2026-11-16]